Turkish Online Journal of Qualitative Inquiry (TOJQI)
Volume 12, Issue 7, July 2021: 9453 – 9478

Research Article

Assessment of Structural Stability and Performance Comparison of Parabolic Trough Collector for Two Different Seasons

Papil M. Gautam[a]*, M.K.Chudasama[b], J.D.Hadiya[c]
[a,b] Assistant professor, of Mechanical Engineering Dept., Government Engineering College, Dahod, India
[c] Student of Mechanical Engineering Dept., Government Engineering College, Surat, India.
Email: [a]gautampapil@gmail.com, [b]mkcgecs@gmail.com, [c]jdhadiya7482@gmail.com

Abstract

This paper gives a wind load simulation model in Siemens NX based on the actual field position of the parabolic trough collector (PTC) when the wind is blowing from multiple directions. The maximum displacement is 0.24 % of the aperture width, and the maximum stress value is 46.51 MPa. Cold airflow computational fluid dynamics (CFD) analysis was conducted to determine the airflow pattern in the vicinity of the PTC. It was revealed that there is no substantial turbulence zone in the area of the receiver tube, which means that heat loss from the receiver tube to the atmosphere will not be increased. The estimated figure of thermal efficiency has a total uncertainty of 1.89 %. The experiment is carried out in March, and the findings are compared to those obtained in December. The results reveal that PTC's thermal performance is better in March. When compared to December, the thermal efficiency of the existing PTC improved by 2.75 % in March. The optimum flow rate for March has been determined to be 3 L/min. The performance of Siemens NX is validated by an experimental result followed by a 0.4 % deviation. Siemens NX is in good agreement with experiment results.

Keywords: *Structural Stability, Performance comparison, parabolic trough, uncertainty analysis, Siemens NX, cold airflow.*

Introduction

Energy is a basic requirement for human survival and evolution. The majority of a country's energy needs are met by commercial sources such as fossil fuels (coal, oil, and natural gas), hydroelectricity, and nuclear power. Energy demand is increasing at an unprecedented rate year after year as living standards rise. On the other hand, fossil supplies are depleting, and the fossil-fuel era is coming to an end. Fossil fuel costs have risen dramatically as a result of growing demand and resource depletion. People are looking for new renewable energy sources to make development more competitive and environmentally friendly. Solar technology has immense potential for satisfying global energy needs, and though solar energy is one of the most promising renewable energy sources, its actual contribution to the globe is still small. Figure 1 shows that a country like India has an annual direct normal sun irradiation potential of around 5.5 kWh/m^2/day. India is one of the world's most solar-power-rich countries.

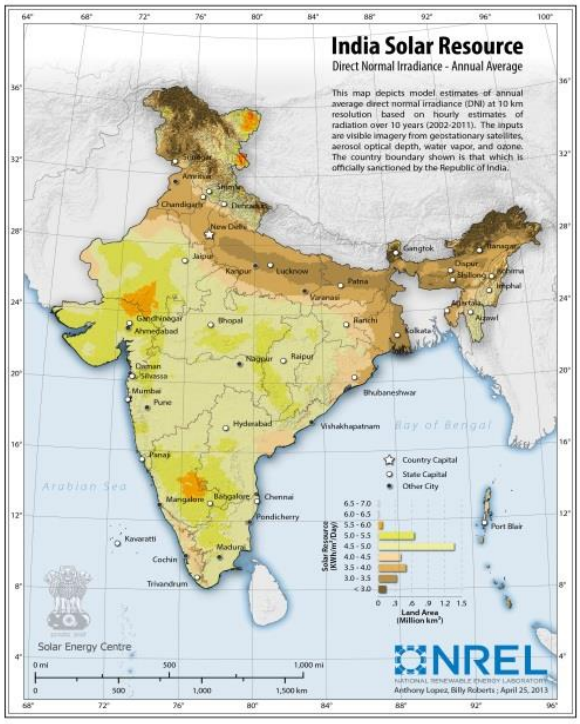

Figure.1.Indian map of Annual Average Direct Normal irradiance[1].

Review Of Related Studies

The applicability of parabolic trough collectors (PTCs) is of great importance among all types of solar systems. **Duffie and Beckman [33]** A parabolic trough collector (PTC) is a line-focus collector that can track the movement of the sun by rotating around a fixed horizontal axis. A parabolic cylinder mirror reflects and concentrates solar energy onto a receiver tube that is aligned with the parabolic cylinder's focal line. The receiver absorbs incoming radiation and converts it to thermal energy, which is collected by a flowing fluid medium within the receiving tube. **A. Fernández-García et al. [2]** divided PTC into two major classes. The first and most evolved plants are concentrated solar power plants (CSP), which are related to the cycles of steam power. The need for low-temperature heat demand and high consumption rates, such as domestic hot water, space heating, swimming pool heating, would be sufficed from the second category. **D.R. Tobergte et al. [3]** described the word "medium temperature collectors" as generally used to describe collectors operating within the 85-250°C range. In 2008, **M. Rommel et al.[4]** clarified that one of the goals of the International Energy Agency's (IEA) Task 33 / IV program for solar industrial process heat was to develop, upgrade and optimize solar thermal collectors for medium temperature. **S.A. Murtuza et al.[5]** suggested better outlet temperatures ranging from 93°C to 103°C were observed from March to May. Experiments were performed at various flow rates of 0.4 L/min, 0.8 L/min, and 1.2 L/min, and the corresponding Reynolds number was measured. It was seen that February to May, compared with other months, gave good surface and outlet temperatures while the fluid flow is laminar. **A.E. Elmohlawy et al. [6]** revealed that the PTC plant's solar thermal energy production achieves 108 MW in summer days with solar field efficiency of 73% and 40 MW in winter with an efficiency of 67%. This energy would be used for steam generation and supplied to power generation or combined power cycle in a traditional steam power cycle. **T.A. Yassen et al. [7]** found that the energy gained from the collector during the summer is 20-60 W/m^2 greater than the energy gained from the collector during the winter. **R. Ait El Cadi et al. [8]** investigated that the solar plant achieves its optimum performance in June with an

increase of efficiency up to 60 % and power output of 3.68 MW for solar irradiation of 936 W/m^2. Spring and full equinox efficiencies should be considered which contributes to better device performance. **J. Wang et al.[9]** illustrated that the parabolic trough solar collectors (PTCs) have varying operating performance and optical efficiency in varying regions and different seasons. **Gopal N. Tiwari et al.[34]** investigated that cooking during peak sunlight hours and space heating in cold climates are both possible with a non-tracking concentrator with a small concentration ratio. Power generating should use a tracking concentrator with a high concentration ratio. **S.A. Kalogirou et al. [12]** finalized the design of a PTC system by optimizing the aperture and rim angle of the collector and choose the diameter of the receiver. Under the ASHRAE 93-1986 (RA91) standard, low-temperature testing of the PTC was carried out by **M. Brooks et al.[13]** with the unshielded and glass-shielded receivers, peak efficiencies of 55.2% and 53.8% were obtained, respectively. **A. Valan Arasu et al.[14]** compared the obtained efficiency equation of the collector with the other literature. The time constant obtained from the test by the collector was 67 seconds. The half acceptance angle of the collector and maximum error tracking are 0.5º & 0.18º, respectively, which means that the collector is operated continuously at the maximum possible performance. **A. Valan Arasu et al.[15]** found that the distortion of the fiberglass reinforced parabolic trough due to wind loading was within reasonable limits against the force applied by a 34 m/s blowing wind. According to ASHRAE Standard 93, the standard deviation of the distribution of parabolic surface errors is calculated as 0.0066 rad. **N. Rosado Hau et al.[16]** investigated a solar-based water heating system where the water heating system reaches a maximum temperature of 55ºC for water as working fluid, and the maximum efficiency of the collector was 5.43 % with a flow rate of 0.022 kg/s at a direct solar irradiance with an incidence angle of 0º. **S. Kalogirou [17]** evaluated the test slope and intercept as 0.387 and 0.638, respectively. The time constant is less than one minute for the collector and the maximum tracking error is 0.2º. **E.Venegas-Reyes et al.[18]** designed PTC for low-enthalpy hot water production with a receiver without a glass cover to reduce both manufacturing and transportation costs, in addition to that finite element stress analysis was conducted to test the PTC's mechanical behavior under different wind loads. **O.A. Jaramillo et al.[19]** designed, constructed, evaluated, and operated five parabolic trough concentrators. Three have been planned with a 90º rim angle, and two have a 45º rim angle. The PTC (45º) and PTC (90º) are having maximum efficiency of 35% and 67 % respectively. In 2014 **G. Coccia et al.[20]** published the paper where the receiver is a circular cross-sectional aluminum pipe that has a glass envelope, as working fluid, demineralized water is used. The results suggest that in the thermal efficiency equation intercept is 0.658 and the slope is 0.6833. **S.M. Arsalan et al.[21]** used a parabola-shaped stainless steel sheet as a reflector in PTC. The receiver consists of galvanized iron pipe and PTC's pick thermal efficiency was 34.71 % with an overall outlet temperature of 57.80ºC obtained at 960 W/m^2 G_b. To produce hot water, PTC is designed, fabricated & assessed. The reflector and receiver are made of acrylic sheet and pure copper respectively. 80ºC was the pick water temperature recorded from the PTC. 52.35% was the overall instantaneous thermal efficiency attended in the work, carried out by **A.K. Pandey et al.[22]**. **Vandana Arora et al.[23]** investigated experimentally the improvements in heat removal factor and collector efficiency based on the test carried out over the year and stated that parabolic trough collector occupies its maximum instantaneous thermal efficiency of 44 % in the summer season. **I. H. Yılmaz et al.[30]** concluded that the mass flow rate requires a lot of pumping effort, so to increase the thermal efficiency of PTC, the optimum mass flow rate is sufficient to sustain it minimally. The receiver's annulus condition has a major effect on thermal efficiency. The best solution for minimizing heat loss is to vacuum the annulus, thus, the use of a less-conducting fluid reduces heat loss through convection through the annulus space. **Sujit kumar verma et al. [32]** presented review paper on cylindrical parabolic reflectors with hybrid phase changing materials (PCM) in an evacuated absorber tube decreases convective and radiation losses from the absorber tube's outer glass surface.

Collectors' receiver portion offers a wide range of design modifications for focusing collectors. The purpose of the various inserts has been to generate turbulence along the flow route in order to increase momentum transfer between the layers of fluid flow and to raise the thickness of the thermal boundary layer in order to increase the rate of energy transfer. Literature review reveals that most researchers have carried out their research for one season. Very limited work has been reported, comparing the experimental performance of the same parabolic trough collector in two different seasons. The position of sun and angle of incidence are also crucial factors which would affect the performance of PTC.

Three fundamental components of the tests conducted and discussed in this paper are novel. (1) With careful examination of such systems, rare relevant literature or experimental data is found for climatic conditions of undeveloped countries, notably in South Asia, such as India. Furthermore, the vast majority of research focuses on high-temperature applications, particularly for power generation, whereas current efforts are primarily focused on low-temperature domestic applications. As a result, the findings provide a useful dataset for future feasibility studies of independent PTC applications in off-grid environments. (2) The developed system described here took advantage of a wide range of local fabrication skills as well as locally available materials. The evaluation of totally local PTC performance under various climatic and operating conditions, adds a lot of significance to these findings, especially for regional growth. (3) The PTC's costly traditional receiver tube is completely replaced with a two-sided open evacuated tube. The thermal efficiency of PTC was experimentally calculated according to the ASHRAE 93-1986 (RA 91) standard**[24]**. PTC’s thermal output can be significantly improved, through manual tracking, rotated about a horizontal E-W axis with continuous adjustment **[25]**.

Design and construction

The purpose of this research is to investigate the performance of existing PTC in March and the results of same will be compared with the performance of collector in December. The collector is designed to fabricate low-cost PTC to decrease expenditure, manufacturing time and minimize the degree of technical ability needed by workshop workers. Several metallic reflector materials were tested by several researchers, and acrylic was found to be the most promising polymer candidate, considering both silver and aluminum as reflective layers**[26].** Commercially available acrylic sheet is used as a reflective surface to minimize manufacturing costs. The parabolic shape for the acrylic sheet was formed by providing the mild steel backup sheet, resting on the ribs framework, and the ribs framework is supported by the mild steel opening frame, as shown in the figure. 2.

Figure.2. Mild steel fabricated structure of PTC.

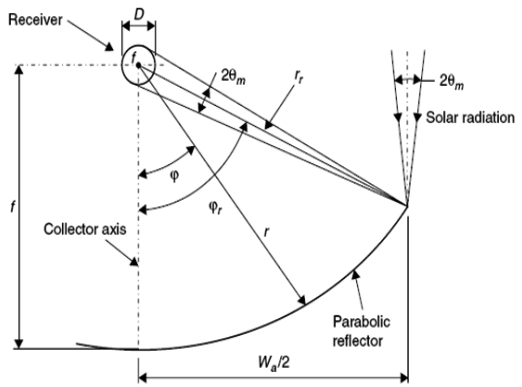

Figure.3. Cross-Section of a circular receiver parabolic trough collector [27].

Based on the available literature certain parameters are selected to finalize the dimension of PTC. Two concentric tubes with a vacuum between the same tubes constitute the solar receiver. The outer diameter and inner diameter of the glass tube are 58 mm and 47 mm respectively, with a thickness of 1.8 mm and 1800 mm is the length of the receiver tube. The collector's experimental thermal efficiency can be determined by Equation (1)**[27].**

$$\eta_t = \frac{mc_p(T_o - T_i)}{A_{ap}G_b} \quad (1)$$

Where, η_t = Thermal efficiency, m = Mass flow rate, G_b = Direct normal irradiance, T_i = Inlet temperature of fluid, T_o= Outlet temperature of fluid. A_{ap} = Aperture area of PTC. Aperture area can be found out by using the thermal efficiency formula.

Aperture area can be calculated by using the thermal efficiency formula.

$$A_{ap} = W_a \times L \quad (2)$$

W_a = Aperture width of a parabola (m), L= Length of a parabola (m), But the receiver length is limited to 1.7 m, putting the value of the length in Equation (2) of aperture area.

$W_a = 1.0\ \text{m}$

Equation (3) gives the parabola equation in terms of coordinates, as shown in the figure. 3.

$$y^2 = 4fx \quad (3)$$

The size of receiver diameter D needed to intercept the entire solar image is defined by Equation (4).

$$D = 2r_r \sin(\theta_m) \quad (4)$$

For this research work, figure. 3 defines the parameters involved in the parabolic profile and provides a detailed explanation of the geometric design of the PTC**[27].** 90º rim angle is chosen because it reduces the mean focus-to-reflector distance and thus reduces the distribution of the reflected beam. The collector's concentration ratio C is defined as the ratio between the aperture area A_{ap} and the receiver area A_r and is expressed by Equation (5).

$$C = \frac{W_a}{\pi D} \quad (5)$$

The parabolic aperture would be calculated by Equation (6).

$$W_a = 4f \tan\left[\frac{\varphi_r}{2}\right] \quad (6)$$

The focal length of the parabolic trough is 0.250 m.

$f = 0.250\ \text{m}$

For parabolic surface construction, the magnitude of the rim angle defines the acrylic material required. The length of the reflective surface curve can be determined by Equation (7) provided by Kalogirou**[27].**

$$S = \frac{H_p}{2}\left\{\sec\left(\frac{\varphi_r}{2}\right)\tan\left(\frac{\varphi_r}{2}\right) + \ln\left[\sec\left(\frac{\varphi_r}{2}\right) + \tan\left(\frac{\varphi_r}{2}\right)\right]\right\} \quad (7)$$

H_p = Latus rectum of the parabola (m) = 1. It is equal to aperture, In the case of 90º rim angle. $S = 1.147\ \text{m}$ the total reflective sheet area essential for construction is, $A = 2.0\ \text{m}^2$. Table 1 provides a summary of all the main features for PTC.

Table.1. A summary of the PTC's main features.

PTCs main feature	
C	5.5
W_a[m]	1
D[mm]	58
f[m]	0.250
H_p[m]	1
φ_r[deg]	90^o
A_{ap}[m^2]	1.70
Collector dimensions	1.00 m × 1.70 m

3.1 Wind load calculation & FEA numerical simulation of wind load by Siemens NX.

Wind load exerted on PTC can be calculated with the use of IS 875, part-3, 1987. The basic wind speed (V_b) for any site can be achieved from the standard **[29].** Design wind speed, V_z at any height z , can be calculated with Equation (8).

$$V_z = V_b \times k_1 \times k_2 \times k_3 \times k_4 \quad (8)$$

Where, k_1=Probability factor, k_2= Height factor, k_3= Topography factor, k_4= Cyclonic region factor. The design wind pressure can be estimated by Equation (9).

$$P_d = K_d \times K_a \times K_c \times P_z \quad (9)$$

$$P_z = 0.6 \times (V_z)^2 \quad (10)$$

k_d = Wind directionality factor, k_a = Area average factor, and k_c = Combination factors are considered in such a way that they represent the actual field condition as given in the standard. The maximum wind load (*F*) exerted by the wind on a parabolic surface can be calculated by Equation (11) specified in Indian wind standard IS 875 – Part- 3,1987.

$$F = C_f \times A_e \times P_d \quad (11)$$

The maximum wind load imposed by the wind on the parabolic surface is approximately 1000 N, calculated according to IS 875-Part 3, 1987. Subsequently, the same value will be considered in all cases for finding the displacement and stress taking place in PTC surfaces. Finite element displacement and stress analysis was performed to evaluate PTC's mechanical behavior. Following are the assumptions made for simulation, (i) Material of PTC is Isotropic. (ii) The relationship between load and deformation is proportional to the stiffness value of the material. (iii) Wind load is assumed to remain constant over the applied surface. (iv) The direction of wind load is not being changed during analysis. Finite elements analysis is based on the displacement process. It's worth noting that this analysis focuses solely on structural resistance to static loads. F_w [N] is the wind load calculated using Equation (12).

$$F_w = \frac{1}{2} \rho_a C_d A_{ap} V_w^2 \quad (12)$$

where ρ_a is the air density, C_d is the coefficient of drag ($1.2 \leq C_d \leq 2.3$ due to the parabolic profile**[19]),** A_{ap} is the PTC aperture area, and V_w is the wind velocity. The maximum wind load was simulated at various PTC positions to assess the structural reliability of the design.

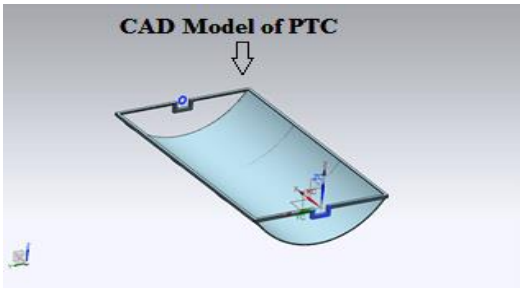

Figure.4. CAD model of PTC.

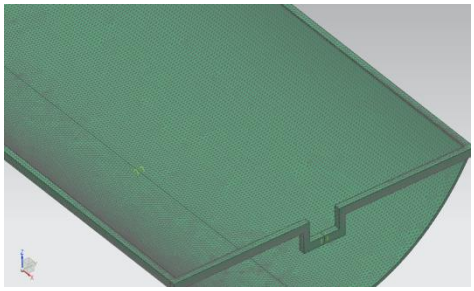

Figure.5. Meshing model of PTC.

Figure. 4 and Figure. 5. Show the current PTCs CAD and mesh model, respectively. For the preparation of the CAD and meshing model, commercially available Siemens NX was used. Tetrahedral 10.00 elements were used to finish the meshing of the parabolic reflective sheet. According to the user guide of software, the performance of such elements is significantly better than the other elements in the same family; further, it will reduce the computational time for a given curve. The entire simulation is divided into 3 parts; each will be treated as a single case. For all three cases, a maximum 1000 N force is considered. These are the maximum possible PTC positions that can be simulated to align the simulation with the field's real condition. In the present work, to check the PTC at its maximum strength, Case-1 is essential, where wind stream attack exactly normal to aperture plane. This wind stream will try to open the parabolic profile surface from the centerline along the longitudinal axis. As shown in Figure. 6.

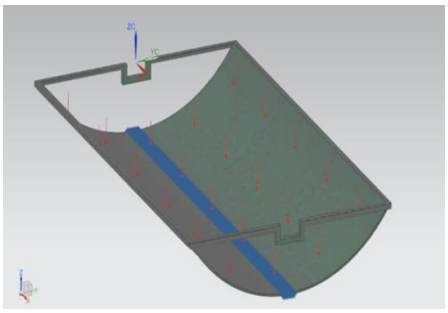

Figure.6. Case-1, wind stream striking from the front opening perpendicular to aperture plane.

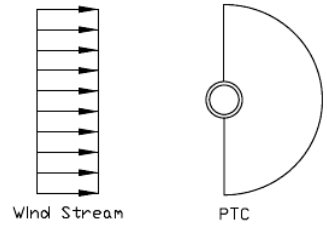

Figure.6.1. Free body diagram of Case-1.

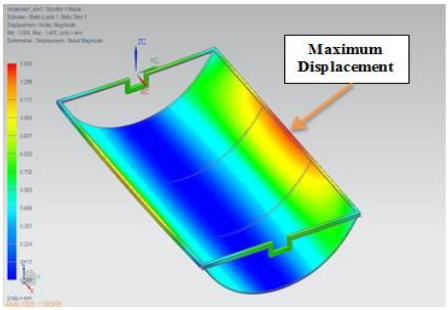

Figure.6.2. Case-1, displacement result of PTC.

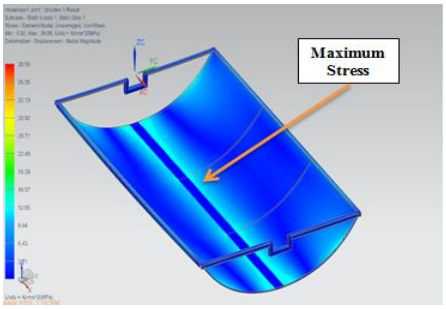

Figure.6.3. Case-1, stress result of PTC.

Figure. 6.2 indicates the maximum displacement value as 1.4 mm, which is within the acceptable limit as compared to its width. Maximum displacement is occurring in the longitudinal direction at the mid-section of the opening frame. Figure. 6.3 shows the maximum stress value of 38.56 MPa, it is also in a tolerable limit of mild steel. Apart from the Maximum stress region, all surfaces of PTC are

experiencing the stress of 3.21 MPa. PTC has been locked $\pm 45^{o}$ hour angle to cater solar radiation between 9.00 am to 3.00 pm. The wind is turned out 45^{o} in simulation instead of PTC to simulate this case. It is better to change wind angle instead of the PTC angle, and this provides ease of simulation operation and gives more realistic results as actual. Figure. 7. describes the actual simulation of this case.

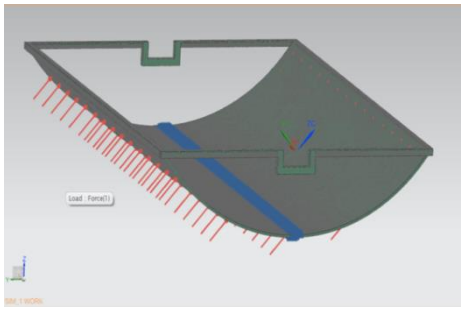

Figure.7. Case-2, wind stream striking from the backside at 45º angle.

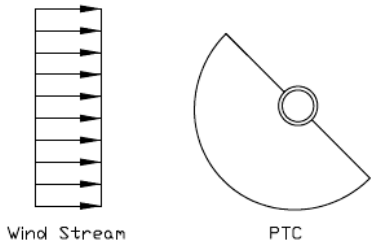

Figure.7.1. Free body diagram of Case-2.

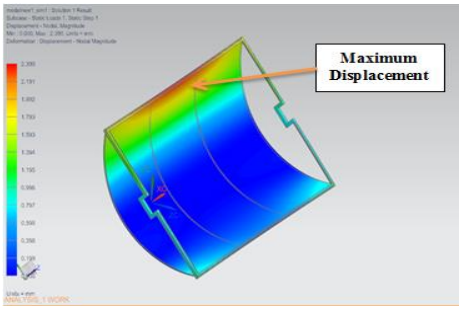

Figure.7.2. Case-2, displacement result of PTC.

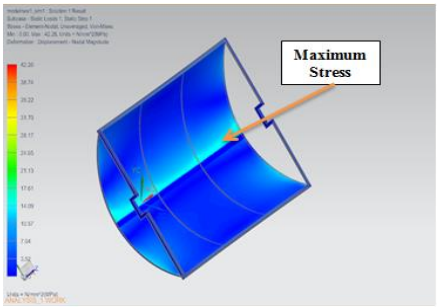

Figure.7.3. Case-2, stress result of PTC.

As shown in the figure. 7.2 maximum displacement value is 2.4 mm. Maximum displacement is taking place in only wind affected portion and the remaining portion are experiencing 0.8 mm and 0.2 mm displacement, respectively. There is no formation of a local slope, which can deflect the sun rays from its focal point, but the same can be taken care of by the receiver. As per figure. 7.3 maximum stress value is 42.26 MPa, which is also within the standard limit of mild steel. PTC has shown quite enough strength to sustain its mechanical properties against this wind load. Case-3 represents the force exerted by the wind when it strikes PTC from the front side at an angle of 45^{o}. The wind is again rotated 45^{o} to simulate this same case. It is beneficial to change the wind angle instead of the PTC angle, and this saves simulation time and provides speedy and more accurate results. Figure. 8 provides the details of the same.

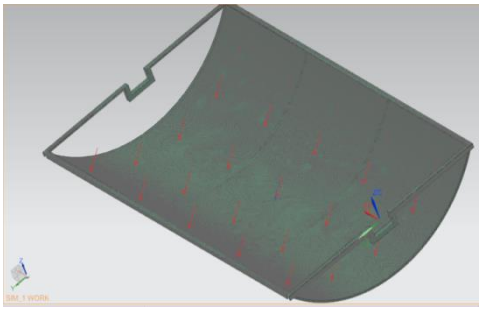

Figure.8. Case-3, wind stream striking from the Front side at 45º Angle.

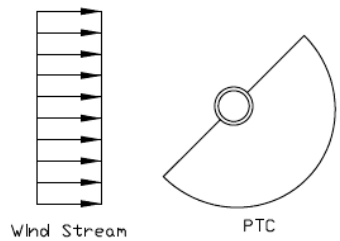

Figure.8.1. Free body diagram of Case-3.

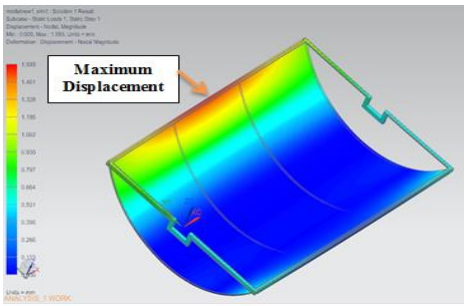

Figure.8.2. Case-3, displacement result of PTC.

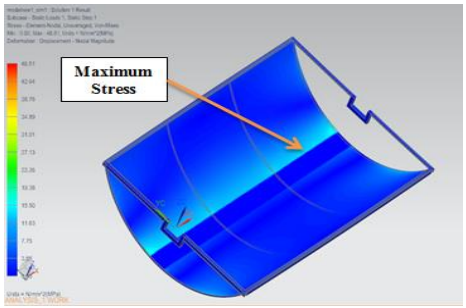

Figure.8.3. Case-3, stress result of PTC.

Figure. 8.2 demonstrates the maximum displacement value as 1.6 mm, which is an acceptable value. The receiver diameter is 58 mm, which is capable of catering to all diverted rays from the local slope. According to figure.8.3, the maximum stress value is 46.51 MPa, the same stress is occurring at the mid-portion of mild steel plate along the receiver axis. The maximum stress value is less than the yield strength of mild steel. This means PTC regains its original position without any permanent deformation. To check the flow pattern of wind flow in the front and backside of PTC, wind flow from different directions is simulated in the following section.

3.2 Cold airflow CFD analysis of parabolic trough collector prototype using Siemens NX.

Cold airflow CFD analysis was conducted to determine the airflow pattern in the vicinity of PTC. It is important to note that identification of different flow patterns like laminar and turbulent will be used to determine the heat loss from the receiver tube to the atmosphere. According to IS 875, part-3, 1987, the basic wind speed of 40.0 m/s for a particular location is taken for all positions. Three positions of PTC for wind flow are identified in which it has to perform in the field, viz. (1) Wind flow from a side face of PTC. (2) Wind flow from Front face at 45^{o} angle of PTC. (3) Wind flow from the backside at 45^{o} angle of PTC.

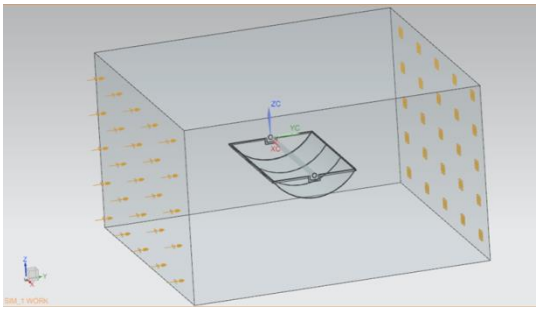

Figure.9. Position -1, Cold Flow boundary conditions.

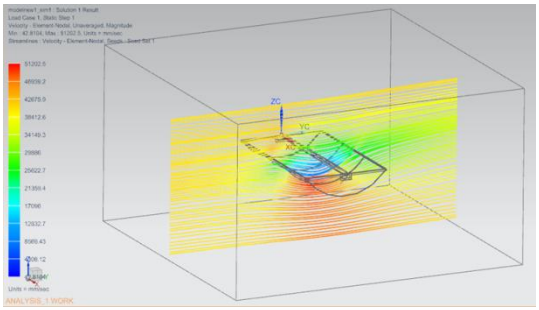

Figure.9.1. Position -1, Cold flow simulation results.

Figure. 9 shows the cold flow boundary condition, PTC is located at the center of the control region, cold air is flowing over the PTC from the left-hand side of the box, and the right-hand side is assigned as an outlet of flow. Under PTC shape, it decreases wind velocity in the vicinity of parabolic shape, which can be identified from Figure. 9.1, and eventually, it reduces heat loss from the receiver. On the backside of the parabolic frame, wind flow is getting accelerate, but it does not render any major effect on the thermal performance of PTC.

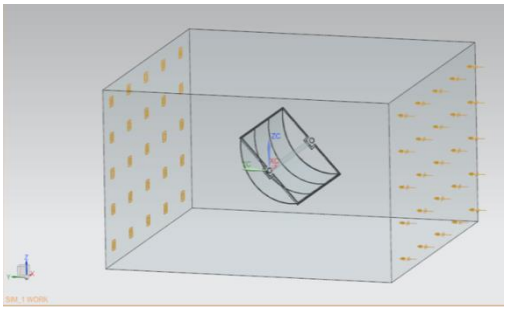

Figure.10. Position-2, Cold Flow boundary conditions.

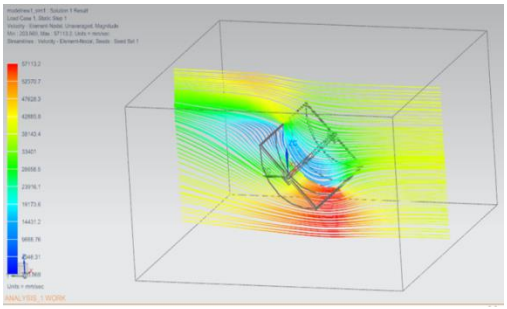

Figure.10.1. Position-2, Cold flow simulation results.

Figure. 10. depicts the cold flow boundary condition, PTC is rotated by 45° at the center of the control region, and the right-hand side is allocated as an inlet of flow while the left-hand side is selected as an outlet. The dimension of the control volume is 5 times larger than the PTC model. It will not give any flow resistance to airflow near its wall. Figure. 10.1. reveals that in the receiver region velocity of air will drop down to 7.0 m/s. It means that PTC is providing great resistance to wind flow in the flowing direction. The value of maximum velocity touched by air in the region of PTC is 57.0 m/s.

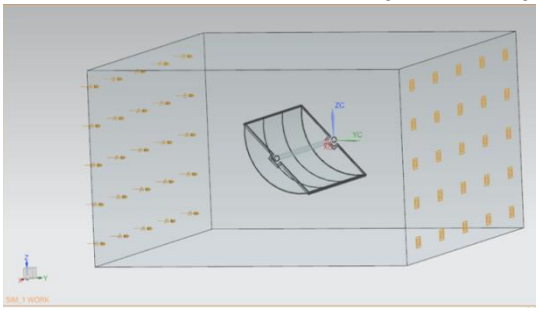

Figure.11. Position-3, Cold Flow boundary conditions.

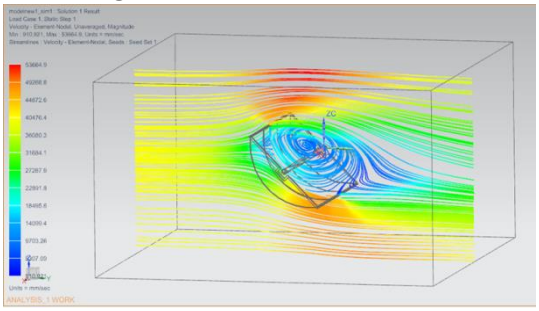

Figure.11.1. Position-3, Cold flow simulation results.

Figure. 11. indicates the cold flow boundary condition. PTC is rotated by 45° at the center of the control region, and the right-hand side is assigned as an outlet of flow. Figure. 11.1. shows that flow is accelerating in the contact region of length side edge, and there is the formation of one low-intensity turbulent zone in the receiver region of PTC. This turbulent zone is low intensity, which does not have any significant effect on the thermal performance of the parabolic trough. Values of maximum and minimum velocity touched by air in the region of PTC are 53.0 m/s and 6.0 m/s, respectively.

Results and Discussion.

4.1 Optical analysis of PTC Model.

The optical efficiency of PTC is known as the energy ratio that the receiver absorbs to the energy incident at the aperture of the collector. Optical performance depends on the optical properties of the materials, the collector's geometry, and the various imperfections resulting from the collector's construction**[27]**, and normally defined by Equation (13).

$$\eta_o = \rho\tau\alpha\gamma\left[\left(1 - A_f \tan\left(\theta\right)\right)\cos\theta\right] \qquad (13)$$

Where ρ is the mirror reflectance, α is the receiver absorptance, τ is the glass cover transmittance, γ is the intercept factor, θ stands for the angle of incidence, and A_f represents the geometric factor. The collector's geometry determines the geometric factor. This is an indication of the successful reduction of the aperture area due to irregular incidence effects, including blockages, shadows, and loss of reflected radiation from the mirror at the receiver end. As represented by Equation (14), the

ratio of the total area lost to the aperture area is known as the geometric factor and is indicated by Kalogirou**[27]**. Figure. 12 shows the actual image of the current research work.

Figure.12. Image of Parabolic trough concentrators.

$$A_f = \frac{A_l}{A_{ap}} \qquad (14)$$

Where A_{ap} is the aperture area of PTC, and total loss in aperture area is denoted by A_l **[27].**

$$A_l = \frac{2}{3} W_a h_p + f W_a \left[1 + \frac{{W_a}^2}{48 f^2} \right] \qquad (15)$$

Where W_a is the PTC aperture width, h_p is the latus rectum, and f is the parabola focal length. The most complex parameter involved in determining the optical efficiency of the PTC is the intercept factor (γ), which is indicated by Equation (16). A simple computer program was developed in MatLab, which numerically evaluates the intercept factor expression.

$$\gamma = \frac{1+\cos(\varphi_r)}{2\sin(\varphi_r)} \int_0^{(\varphi_r)} \frac{erf(M) - erf(N)}{[1+\cos(\varphi)]} d\varphi \qquad (16)$$

Where erf () is the "error function" of M and N indicated by

$$M = \frac{\sin(\varphi_r)\left[1+\cos(\varphi)\right]\left[1-2d^* \sin(\varphi)\right] - \pi\beta^* \left[1+\cos(\varphi_r)\right]}{\sqrt{2}\pi\sigma^* \left[1+\cos(\varphi_r)\right]}$$

$$N = -\frac{\sin(\varphi_r)\left[1+\cos(\varphi)\right]\left[1+2d^* \sin(\varphi)\right] + \pi\beta^* \left[1+\cos(\varphi_r)\right]}{\sqrt{2}\pi\sigma^* \left[1+\cos(\varphi_r)\right]}$$

d^* is the universal nonrandom error parameter because of receiver mislocation and reflector profile errors $(d^* = d_r / D)$, β^* is the universal nonrandom error parameter due to angular errors $(\beta^* = \beta C)$, σ^* is the universal random error parameter $(\sigma^* = \sigma C)$, C is the ratio of collector concentration (A_{ap} / A_r), D is the receiver external diameter, d_r is the receiver displacement from the focus axis, and misalignment angle error is denoted by β. Measuring the standard deviation of the total reflected energy distribution at normal incidence, random errors σ can be statistically modeled by Equation (17)**[27].**

$$\sigma = \sqrt{\sigma_{sun}^2 + 4\sigma_{slope}^2 + \sigma_{mirror}^2} \qquad (17)$$

In table 2, the optical efficiency η_o and all other parameters involved in the optical efficiency equation are listed. Optical efficiency η_o is calculated by considering the angle of incidence θ as zero.

Table 2. The optical parameters for PTC.

$\eta_o[-]$	0.64
$A_f[-]$	0.5882
$\rho[-]$	0.90
$\tau[-]$	0.80
$\alpha[-]$	0.93
$\gamma[-]$	0.96

By comparing the optical performance of the current PTC prototype with the optical performance provided in the literature, it can be concluded the optical performance of the PTC prototype is worthwhile. The optical efficiency η_o is shown in figure. 13 as a function of the angle of incidence θ . It is obvious from the figure that the optical efficiency η_o strongly depends on the angle of incidence θ . At the zero angles of incidence, the optical efficiency value is maximum, as the incidence angle value increases and the optical efficiency value decreases. Both are inversely proportioned to one another.

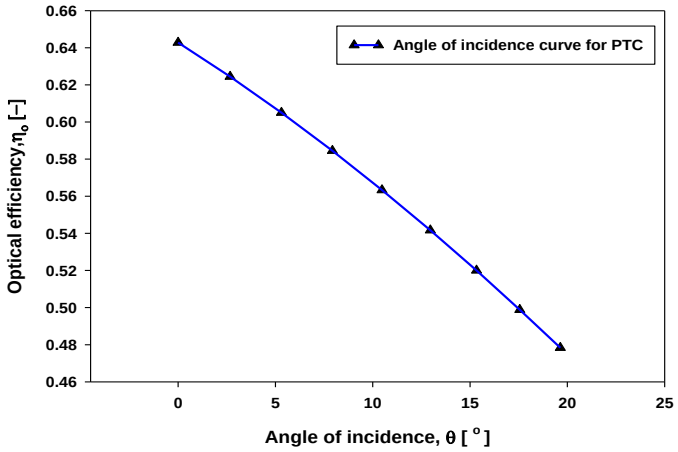

Figure.13. PTC's optical efficiency is a function of the incidence angle.

4.2 Thermal performance of PTC Model.

According to the ASHRAE 93-1986(RA 91) standard, the thermal efficiency of PTC has been experimentally evaluated. In section 8.2.1.1 of the ASHRAE 93 1986 (RA 91) standard, a test method for determining the thermal efficiency of a concentrative collector is specified. To evaluate the time constant, the instantaneous thermal efficiency and the incidence angle modifier outdoor experiment were carried out in March at Surat, Gujarat, India (21°10'45.8"N, 72°48'47.6"E)**[24].**

4.2.1 Time constant

A collector's time constant is the time taken by the leaving fluid to achieve 63.2 % of its final steady value, followed by a step-change in direction of incident radiation. It can be obtained by the test suggested by standard ASHRAE 93-1986 (RA 91)[24]. PTC's time constant for the heating can be calculated by solving Equation (18).

$$\frac{T_o - T_{o,t}}{T_o - T_i} = \frac{1}{e} = 0.368 \quad (18)$$

Where T_o is the final outlet water temperature of the collector, T_i is the inlet water temperature, and $T_{o,t}$ is the outlet water temperature of the collector after a time t. In the heating test, the inlet temperature of the collector was maintained equal to the ambient temperature, initially at the defocused position and then abruptly shifted to the focused position. To obtain the time constant during cooling conditions the collector is also operated with the fluid inlet temperature maintained at the ambient temperature. The solar energy is suddenly reduced to zero by defocusing the collector. As a function of time, the transfer fluid temperatures are monitored constantly until Equation (19) is satisfied.

$$\frac{T_{o,t} - T_i}{T_{oi} - T_i} = \frac{1}{e} = 0.368 \quad (19)$$

Where, T_{oi} is the collector outlet water temperature at initial. The constants of heating and cooling are described in table 3.

Table 3. The time constant for heating and cooling conditions.

	Time constant	
	Heating	Cooling
PTC	34.7 s	55.80 s
	T_i = 34.50 ^{o}C	T_i = 34.50 ^{o}C
	T_o = 40.37 ^{o}C	T_{oi} = 40.37 ^{o}C
	$T_{o,t}$ = 38.20 ^{o}C	$T_{o,t}$ = 36.66 ^{o}C

4.2.2 Thermal efficiency.

In this present work, experimentation is carried out in March near to equinox in a close circuit. figure. 14 displays line layout of setup. The same working fluid would be re-circulated at any point of time in the close cycle. There is one working fluid reservoir tank which supplies working fluid to the parabolic trough receiver through the supply pump. The mechanical stirrer is provided for proper fluid mixing to get even temperature distribution. Using the Rotameter with a control knob can be used to adjust the working fluid mass flow rate. In addition to control the mass flow rate of the working fluid, a by-pass arrangement valve is also provided. Two temperature sensors are mounted, one at the inlet and one at the outlet portion of the working fluid to measure the inlet and outlet temperature, respectively. Two separate sensors will measure the receiver tube skin temperature and skin temperature of the reflective sheet, and one individual sensor is provided for ambient temperature measurement. All of these temperature sensors are PT-100 types calibrated and finally, the signals are connected to a computer for observation.

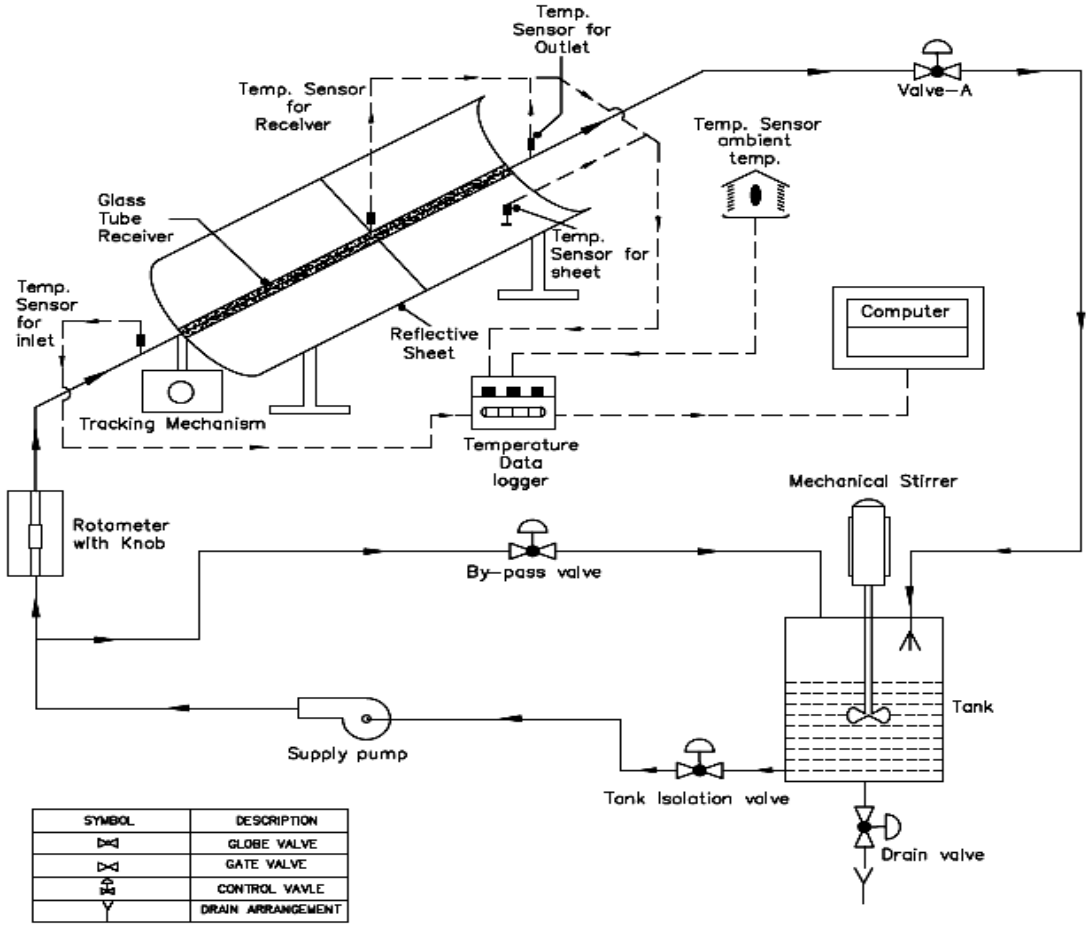

Figure.14. Schematic line layout of the PTC test setup.

To run an efficiency test according to the ASHRAE 93-1986 standard requires a duration equal to one time constant time or 5 minutes, whichever is greater**[24]**. The thermal instantaneous efficiency of a PTC η_t is defined as the ratio of useful energy supplied to the fluid for heat transfer to the energy obtained from the collector's aperture area. The thermal efficiency of PTC can be estimated by using Equation (1)**[27]**

$$\eta_t = \frac{mc_p(\mathrm{T_o} - \mathrm{T_i})}{A_{ap}G_b}$$

The thermal efficiency of concentrators is provided by Kalogirou[17] through the First Law, as given by Equation
(20).

$$\eta_t = F_R\left[\eta_o - \frac{U_L}{C}\left(\frac{\Delta T}{G_b}\right)\right] \qquad (20)$$

Where, $\Delta T = \left(T_i - T_a\right)$, η_o is the PTC's optical efficiency at a normal angle of incidence of, F_R is heat removal factor, U_L is the overall loss coefficient. If instantaneous thermal efficiency η_t is plotted against the functional term $(\Delta T / G_b)$. The outcomes are linearly connected, thus, the right-hand side of equation 16 will be considered a straight line with intercept a and slope b. The instantaneous thermal efficiency of a PTC is likely to be given in the form of a linear equation, consequently, the thermal efficiency equation can be written as Equation (21)**[17].**

$$\eta_t = a + bT^* \quad (21)$$

$$a = F_R\eta_o$$

$$b = -F_R U_L / C$$

$$T^* = (\Delta T / G_b)$$

Where a is y-intercept and b is the slope of a line. It is essential to mention that $F_R\eta_o$ and $F_R U_L / C$ are almost constant for a collector operating under steady irradiation and liquid flow rate condition **[27],** Owning to single-axis tracking in the present research, it is not possible to maintain 0^o angle of incidence at every point of time, which gives an inclined line with the negative slope in efficiency curves. Figure. 15 shows the efficiency curves of PTC in March. To obtain thermal efficiencies for solar concentrators, A straight line of best fit can be drawn through these points indicating the thermal efficiency. It should be noted that the linear fit is used instead of the 2nd degree to find an acceptable relationship between η_t and $(\Delta T / G_b)$. 71.0 % is the maximum efficiency value touched by the PTC in this test with a 3 L/min flow rate. All the calculated and concerned thermal parameters are reported in Table 4.

Table 4 . Thermal performance of PTC in December and March.

	December 2019	**March 2020**
$U_L[W/m^2K]$	19.67	15.91
$F_R[-]$	0.946	0.963
$C[-]$	5.5	5.5
$\eta_t[-]$ at 3 L/min	$0.6053 - 3.3831\left(\Delta T / G_b\right)$	$0.6165 - 2.7878\left(\Delta T / G_b\right)$
$\eta_o[-]$	0.64	0.64

It is found from the thermal performance of PTC, on March 3 L/min flow rate achieves quite well results as compared to another flow rate of experiment. It is selected as the optimum flow rate for the existing test setup of PTC. In the case of 3 L/min, the nature of thermal efficiency curves comparatively more constant.

The higher value of the Heat removal factor (F_R) in March compared to December points out the actual useful energy gain is higher in March. The higher value of the overall loss coefficient (U_L) indicates lower heat resistance, and it shows a high quantity of heat loss from the PTC receiver to the atmosphere. The value of the overall loss coefficient (U_L) in December is higher as compared to March. To summarize the performance of the existing PTC in both months, it is clear from the thermal outcomes parameters that the performance of PTC in March is better than in December month.

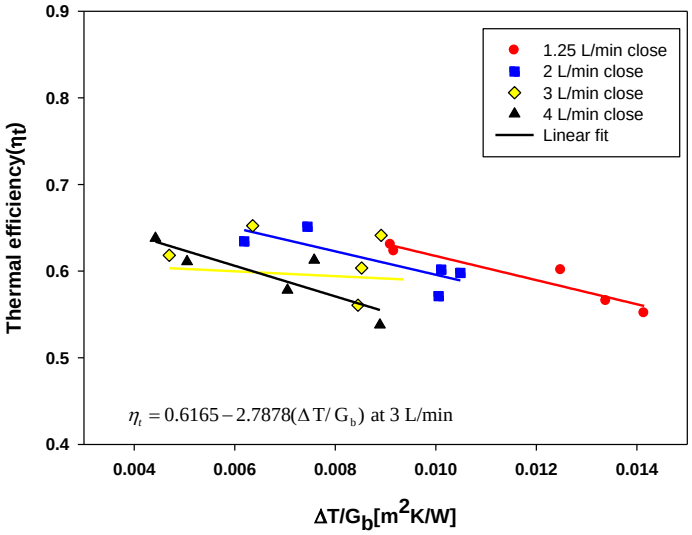

Figure.15. Experimental results data and best-fit curve for the PTC in March.

The variations of the ambient data for 3 L/min in ambient temperature and wind speed are given in Figure. 16. The data was recorded using the PT-100 type thermometer and the digital anemometer AVM-03, respectively.

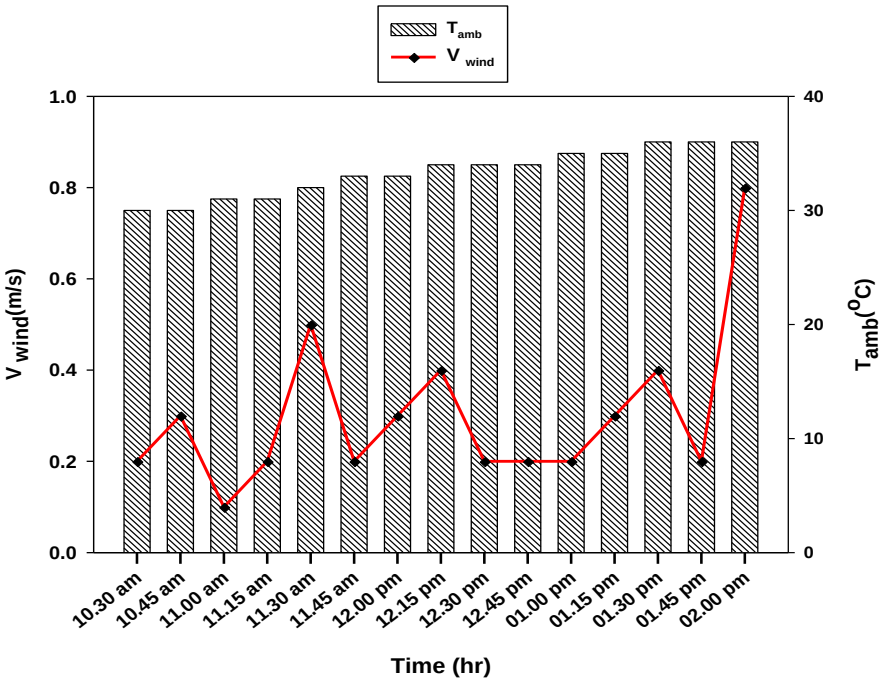

Figure. 16. Wind speed and ambient temperature for 3 L/min in March.

Using a solar meter (MECO-936) with 20 reading storage facilities, direct solar radiation was reported and the average G_b values during the investigation are shown in the figure. 17.

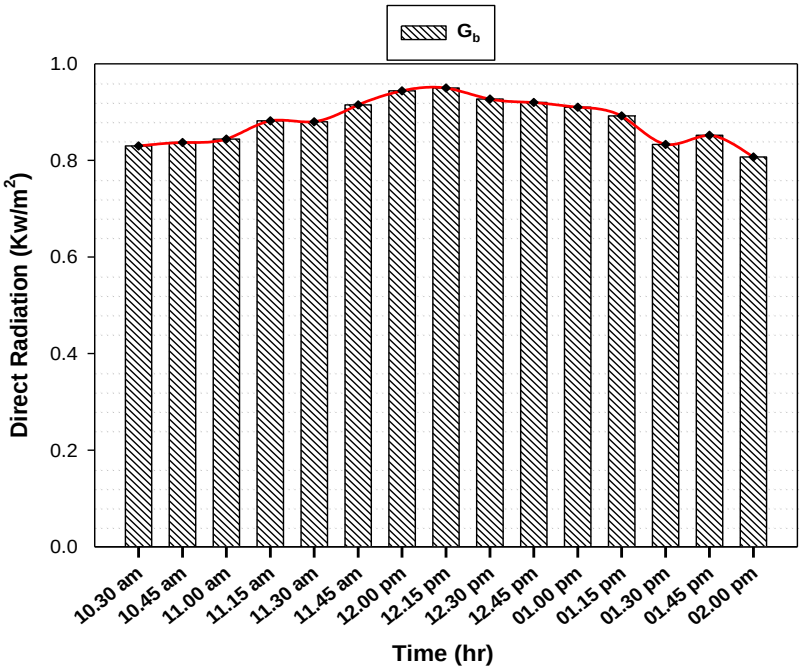

Figure.17. The average value of G_b for 3 L/min in March

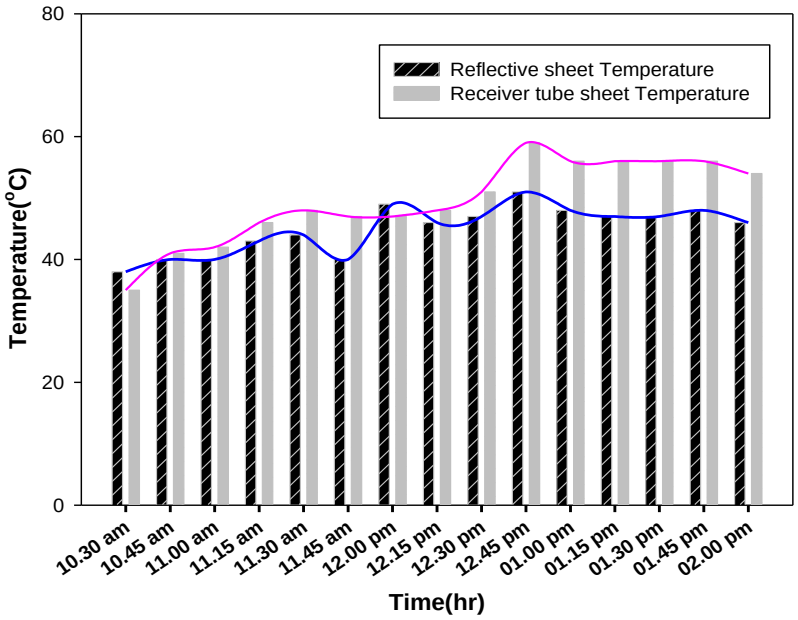

Figure.18. Reflective sheet and receiver tube temperature variation for 3 L/min in March.

Figure. 18 shows the variation in reflective sheet and receiver tube temperature during experimentation, excluding two points 10.30 am and 12.00 pm, at almost points receiver tube temperature is higher, which can lead to heat loss from the tube to the atmosphere and it can also improve the heat transfer rate to working fluid. Reflective sheet temperature is also within the safe limit of touch during experiments.

4.2.3 Incidence angle modifier.

This is simply a factor of correlation added to the curve of efficiency. Because of the change in incidence angle, the incidence angle modifier defines the drop in optical efficiency. The optical efficiency in Equation (13) is highly dependent on the incidence angle. The incidence angle modifier is a function of just the angle of the incident between the direct solar beam and the outer normal to the

aperture plane of the collector. It explains how the collector's optical performance changes as the angle of the incident changes. The incidence angle modifier K_θ is well-defined by using Equation (22).

$$K_\theta = \frac{\eta_t \left(T_i = T_a\right)}{F_R\left[\eta_o\right]} \qquad (22)$$

The incidence angle modifier is calculated according to ASHRAE Standard 93-1986, Section 8.3.4.2.2, and Method 2. Figure. 19. shows the incidence angle modifier as a function of the incidence angle.

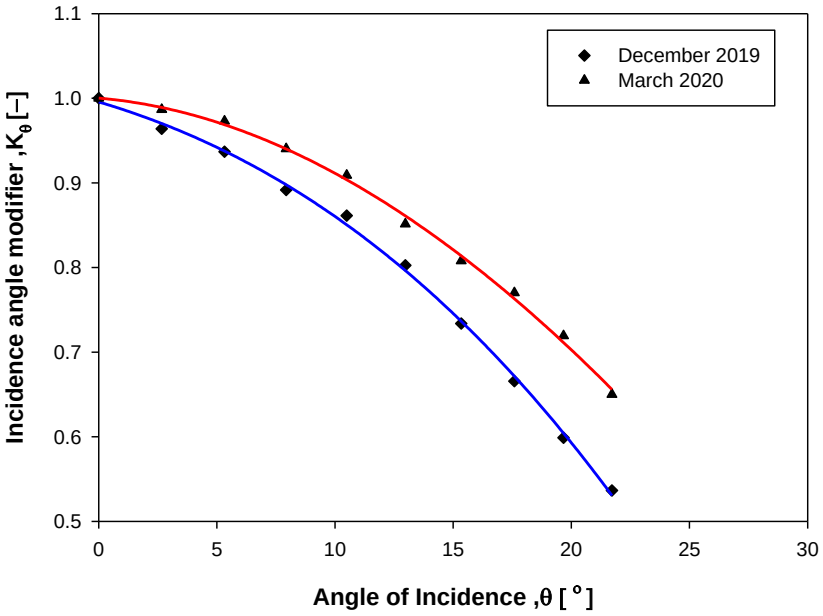

Figure.19. Incidence angle modifier curves of PTC in December and March.

The regression analysis for the incidence angle modifier in March and December is reported in Table 5. These equations of incidence angle modifiers are calculated by using a curve fitting method (Second-order polynomial fit**)[17].**

Table 5. Regression analysis of the incidence angle modifier in December and March.

	K_θ
December 2019	$K_\alpha = 6.528\times10^{-6}\theta^3 - 5.096\times10^{-4}\theta^2 - 1.285\times10^{-2}\theta + 1.005$
March 2020	$K_\alpha = 4.771\times10^{-6}\theta^3 - 2.062\times10^{-4}\theta^2 - 1.18\times10^{-2}\theta + 1.008$

4.2.4 Uncertainty Analysis.

Analysis of uncertainty is necessary to prove the exactness of the experiments. Errors also come from the sensitivity of the equipment and measurements. Holman**[28]** carried out the uncertainty analysis of the various measured and estimated Parameters. For the present work experimentation is performed daily from 10:30 am to 02:00 pm in March-2020. Operating temperatures were measured using PT100 RTD with a measuring temperature range from -40°C to 85 ° C with a precision of ± 0.1°C.

Whereas climate data including wind speed and solar radiation were measured using a digital anemometer AVM-03 and a solarimeter (MECO-936) and the accuracy of the anemometer is ± 3 %, and for solarimeter, it is ± 10 w/m^2. The uncertainty in the output parameter, i.e., thermal efficiency, is

determined as follows using the root sum square method Equation (23)**[28]**. The total uncertainties of the instruments are given in Table 6.

If $y = f(x_1, x_2, x_3, x_4, x_5, x_6, x_7, ...)$

$$W_y = \sqrt{\left(\left(\frac{\partial y}{\partial x_1} Wx_1\right)^2 + \left(\frac{\partial y}{\partial x_2} Wx_2\right)^2 + \left(\frac{\partial y}{\partial x_3} Wx_3\right)^2 + ...\right)} \quad (23)$$

Table 6. Uncertainties of the instruments.

Sr. No.	Measurements	Type	Uncertainty
1	Temperature	PT 100 RTD	± 0.1 ° C
2	Velocity	Digital anemometer	± 3 %
3	Water flow rate	Rotameter	± 3 %
4	Radiations	Handy solarimeter	± 10 w/m^2
5	Reaction time	Digital stopwatch	0.2 sec

The total uncertainty in the measured value of thermal efficiency is 4.85 %.

Validation of a numerical simulation model by experimental performance.

An attempt was made to develop one Siemens NX thermal model to be validated by experimental performance. Every position of PTC and Sun location are independently simulated by considering actual data from inputs, also different PTC positions and the location of the sun at that particular time are individually simulated to compensate for the tracking mechanism. For the accuracy of the software under real field conditions, convection heat loss from the PTC receiver tube to the atmosphere is also integrated into this simulation. As mentioned in the previous section 4.2.1 of thermal efficiency, PTC shows its best thermal performance at 3 L/min in March. Thermal performance at 3 L/min only has been taken for validation and will be compared with a thermal performance at 3 L/min in December. Following assumptions are made during the simulation, (i) There is no thermal loss from the outlet coupling surfaces. (ii) In an individual simulation, the minimum angle of incidence is considered. (iii) A constant solar irradiation value, distributed uniformly along the length of the receiver tube, is assumed for individual simulation. (iv) Across the length of the receiver tube, a zero pressure gradient is assumed. (v) The flow at the receiver inlet has a uniform velocity.

The CFD modeling approach involves continuity Equation (24), momentum Equation (25), and energy balance Equation (27) for turbulent flow **[31].**

Continuity equation:

$$\frac{\partial p}{\partial t} + \nabla \cdot (\rho \vec{v}) = 0 \quad (24)$$

Where $\vec{v}$ is the velocity vector, ρ is a density.

Momentum equation:

$$\frac{\partial}{\partial t}(\rho \vec{v}) + \nabla \cdot (\rho \vec{v}\vec{v}) = -\nabla P + \nabla \cdot (\bar{\bar{\tau}}) + \rho \vec{g} \quad (25)$$

Where P is the pressure, $\bar{\bar{\tau}}$ is a stress tensor, and $\rho \vec{g}$ is the gravitational body force. The stress tensor is represented by

$$\overline{\overline{(\tau)}} = \mu\left[\left(\nabla\vec{\upsilon} + \nabla\vec{\upsilon}^{T}\right) - \frac{2}{3}\nabla.\vec{\upsilon}I\right] \qquad (26)$$

Energy equation:

$$\frac{\partial}{\partial t}(\rho E) + \nabla\cdot(\vec{v}(\rho E + p)) = \nabla\cdot(k_{eff}\nabla T - \sum_{j} h_j \overrightarrow{J_j} + (\overline{\overline{\tau}}_{eff}\vec{v})) + S_h \qquad (27)$$

Where k_{eff} it represents the effective thermal conductivity. $\overrightarrow{J_j}$ is the diffusion flux of species J. The first three terms on the right-hand side of Equation (27) are for energy transfer due to conduction, species diffusion, and viscous dissipation respectively, and S_h contains all the volumetric heat sources. In Siemens NX, the CAD model of the PTC with a receiver tube was prepared, as shown in the figure. 20. Meshing was performed after the completion of the modeling operation. Figure. 21 display a clear view of the mesh model. The meshing of the parabolic reflective sheet was completed with Quad 4 thin shell elements. According to information available in the user guide of software, performance of said elements is quite better than the other elements of the same family; in addition to that, it will also reduce the computational time for a given curve. Figure. 22 indicates the thermal coupling between the reflective sheet and the receiver tube. The concept of the thermal constraint is also applied between the receiver tube and the surrounding atmosphere.

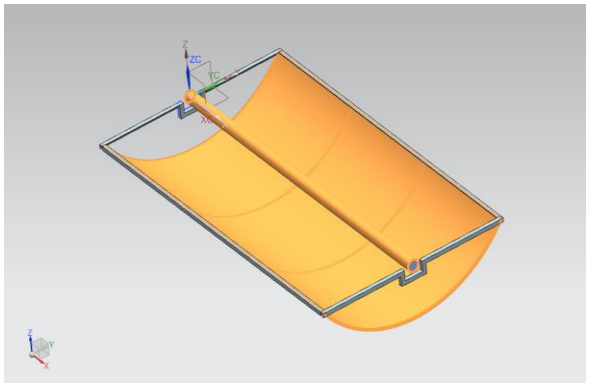

Figure.20. CAD model of PTC with a receiver in simulation

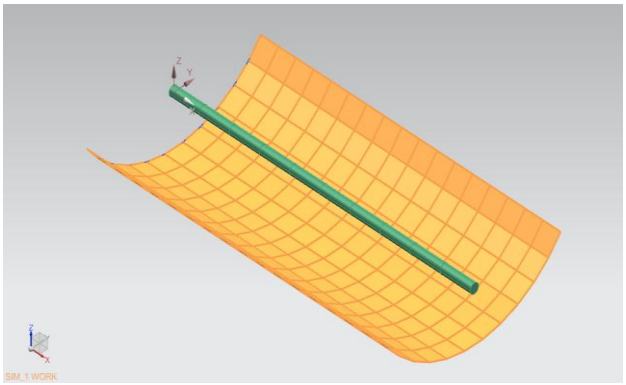

Figure.21. Mesh model of PTC in simulation

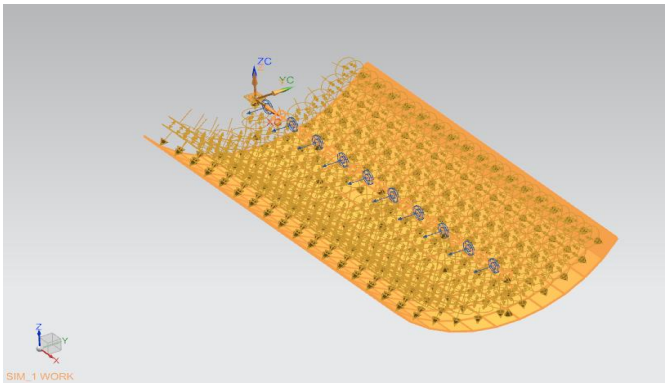

Figure.22. Applied thermal coupling and constrain in simulation.

Figure. 23 displays the effects of the thermal simulation in March. Simulation of the PTC was performed under real environment and inlet conditions. To make this simulation run more reliably, all individual PTC positions are simulated separately. For 3 L/min three selective points were taken to validate software reading, i.e. 10.00 am (Start point), 12.45 pm (Maximum efficiency), and 14.00 pm (Endpoint). $T_{o,\,NX}$ represents the outlet temperature of working fluid calculated by the software and $T_{o,\,Exp.}$ shows the outlet temperature of working fluid achieved during the experiment. To calculate the thermal efficiency for Siemens NX, the outlet temperature of the water must be obtained, since the

remaining values in thermal efficiency Equation (1) are already known. The final results of Siemens NX are suggesting strong agreement with the data from the experiment.

Figure. 24 indicating collective graph of thermal efficiency and Siemens NX thermal efficiency with the angle of incidence in March. In March maximum efficiency is occurring at 12.45 pm, which is near to solar noon condition. As indicated in the figure. 16 & 17 velocities of wind are the approach to a minimum value and the value of G_b is much closer to its maximum value at 12.45 pm.

This indicates minimum heat loss from the receiver to the atmosphere and maximizes the possibility of the working fluid heat gain. At 12.45 pm the difference in both efficiencies is 0.4 % only. From 10.30 am to 12.45 pm both efficiencies are very close to each other, while a higher value of angle of incidence(AOI), after 12.45 pm deviation increased to 5 %. However, still, all these differences are within the acceptable limit of efficiency. AOI forms the shape of the cone in the graph, Siemens NX thermal efficiency showing a good agreement with the experimental efficiency inside the cone angle of incidence.

10.30 AM

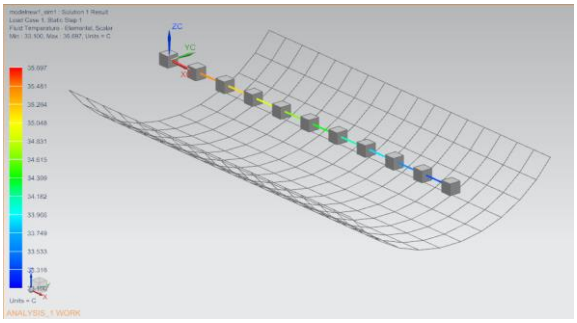

$T_{o,NX}$ =35.69ºC / $T_{o,Exp.}$ =35.60ºC

14.00 PM

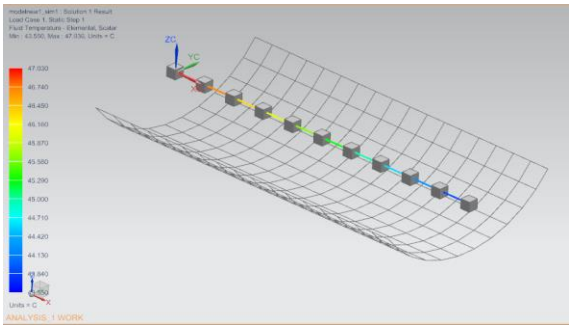

$T_{o,NX}$ =47.00ºC / $T_{o,Exp.}$ =46.90ºC

12.45 PM

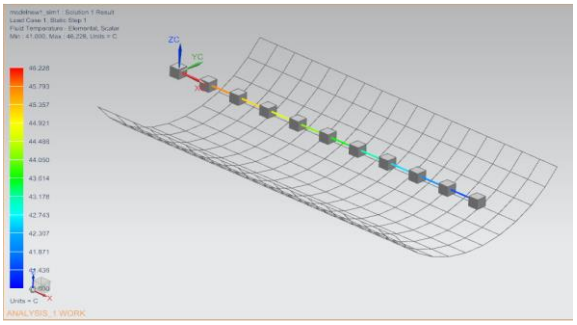

$T_{o,NX}$ =46.22ºC / $T_{o,Exp.}$ =46.20ºC

Figure.23. Simulation results for a close circuit in March.

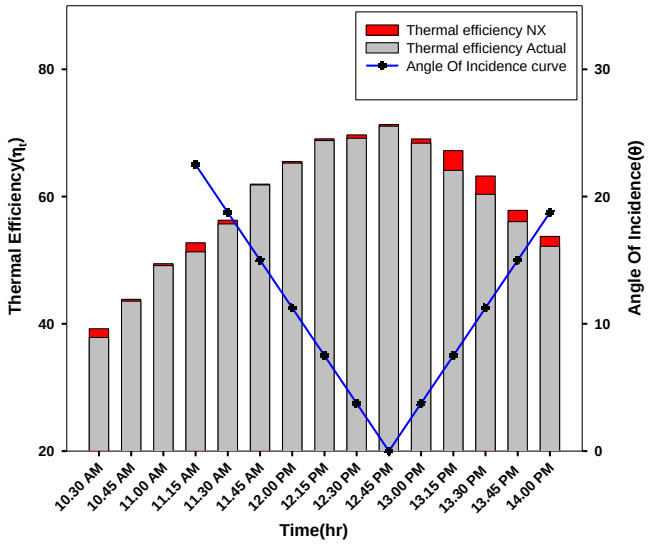

Figure.24. Experimental and Siemens NX thermal efficiency comparison with AOI in March.

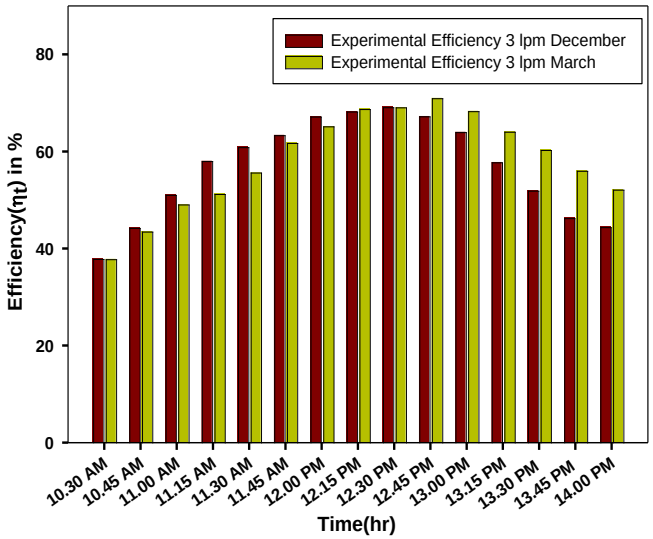

Figure.25. Experimental thermal efficiency comparison in March & December.

Figure. 25. Presents the experimental thermal efficiency comparison for both mentioned months. Efficiencies in December from 10.30 am to 12.00 pm is comparatively higher and from 12.15 pm to 12.30 pm it is almost equal to March. At 12.45 pm PTC efficiency touches its maximum value for March, afterwards, efficiency sustains its higher value till 14.00 pm in March. Owing to the smaller value of angle of incidence in March, the overall thermal performance of PTC is worthy in March (Near to equinox) as compared to December.

Conclusions

Numerical simulation of the PTC model is carried out in different possible flow directions with a maximum wind load of 1000 N. It has been observed that among all the conditions of loading maximum displacement value occurs in case-3 as 2.4 mm. The structure of PTC is showing enough strength against maximum wind load. In all cases, maximum stress values are well within the yield

strength of mild steel value. There is no possibility of local slope formation, which could deteriorate the thermal performance of PTC. In addition to that, it would also improve the opportunity to intersect reflected rays coming from the reflector.

The design of PTC does not support the formation of a high-intensity turbulent zone in the vicinity of the receiver tube. It leads to low heat loss from the receiver tube to the atmosphere. The overall uncertainty in the thermal efficiency calculated value is 1.89 %. The fabrication cost of PTC is approximate 148 US$ per square meter which is 14.11 % less as compared to other PTC[19] of the same aperture area and it is significantly less. As compared to December the value of the Heat removal factor is being improved by 1.8 % and the overall loss coefficient value is reduced by 19.11 % in March, because of that the pick experimental thermal efficiency is increased by 2.75 % for existing PTC in March compared to December.

The thermal efficiency simulation of Siemens NX with a volume flow rate of 3 L/min was conducted in March, showing strong agreement with the experimental thermal efficiency within the specific angle of incidence scale. At an optimal flow rate, the minimum and maximum deviations of Siemens NX efficiency from experimental efficiency are 0.4 % and 5 % respectively. The simulation model would be used to predict the thermal behavior of a similar type of PTC.

5.1 Future scope of the study.

Future researches can be directed towards the following study:

- PTC can be operated near equinox conditions to compare its performance with another season.
- Phase-changing material (PCM) can be used as a heat storage device to provide heat in off time.
- Various types of nanofluid with the hybrid combination can be employed in place of a normal working fluid to enhance the thermal performance of PTC.
- PTC can be arranged in a series manner to suffice higher temperature and high flow rate application demand.

References

[1] N. Cell, India Solar Resource Data : Hourly, (2012) 1–2. nrel.gov/international/ra_india.html.

[2] A. Fernández-García, E. Zarza, L. Valenzuela, M. Pérez, Parabolic-trough solar collectors and their applications, Renew. Sustain. Energy Rev. 14 (2010) 1695–1721.

[3] D.R. Tobergte, S. Curtis, Potential for Solar Hear in Industrial Processes, J. Chem. Inf. Model. 53 (2013) 1689–1699.

[4] Weiss W, Rommel M. Solar heat for industrial processes, medium temperature collectors. State of the Art within Task 33/IV, Subtask C. Solar Heating and Cooling Executive Committee of the International Energy Agency; 2005.

[5] S.A. Murtuza, H.V. Byregowda, M.M.A. H, M. Imran, Experimental and simulation studies of parabolic trough collector design for obtaining solar energy, Resour. Technol. 3 (2017) 414–421.

[6] A.E. Elmohlawy, B.I. Kazanjan, V.F. Ochkov, Modeling and performance prediction of solar parabolic trough collector for hybrid thermal power generation plant under different weather conditions, AIP Conf. Proc. 2047 (2018).

[7] T.A. Yassen, Experimental and Theoretical Study of a Parabolic Trough Solar Collector, Anbar Journal for Engineering Sciences. 5 (2012) 109–125.

[8] R. Ait El Cadi, Power Generation and Heating Performances of An Organic Rankine Cycle Driven by Parabolic Trough Collectors, Int. J. Eng. Res. V8 (2019) 115–120.

[9] J. Wang, J. Wang, X. Bi, X. Wang, Performance Simulation Comparison for Parabolic Trough Solar Collectors in China, Int. J. Photoenergy. 2016 (2016).

[10] Murphy LM, May EK. Steam generation in line-focus solar collectors: a comparative assessment of thermal performance, operating stability, and cost issues 1982. SERI/TR-632-1311.

[11] Hurtado P, Kast M. Experimental study of direct in-situ generation of steam in a line focus solar collector 1984. DOE/SF/11946-T1.

[12] S.A. Kalogirou, S. Lloyd, J. Ward, P. Eleftheriou, Design and performance characteristics of a parabolic-trough solar-collector system, Appl. Energy. 47 (1994) 341–354.

[13] M. Brooks, I. Mills, T. Harms, Design, construction and testing of a parabolic trough solar collector for a developing-country application, Proc. Sol. World Congr. 2005 Bringing Water to World, Incl. Proc. 34th ASES Annu. Conf. Proc. 30th Natl. Passiv. Sol. Conf. 2 (2005) 849–854.

[14] A.V. Arasu, T. Sornakumar, Performance characteristics of parabolic trough solar collector system for hot water generation, Int. Energy J. 7 (2006) 137–145.

[15] A. Valan Arasu, T. Sornakumar, Design, manufacture and testing of fiberglass reinforced parabola trough for parabolic trough solar collectors, Sol. Energy. 81 (2007) 1273–1279.

[16] N. Rosado Hau, M.A. Escalante Soberanis, Efficiency of a parabolic trough collector as a water heater system in Yucatn, Mexico, J. Renew. Sustain. Energy. 3 (2011).

[17] S. Kalogirou, Parabolic Trough Collector System for Low Temperature Steam Generation: Design and Performance Characteristics, Appl. Energy. 55 (1996) 1–19.

[18] E. Venegas-Reyes, O.A. Jaramillo, R. Castrejón-García, J.O. Aguilar, F. Sosa-Montemayor, Design, construction, and testing of a parabolic trough solar concentrator for hot water and low enthalpy steam generation, J. Renew. Sustain. Energy. 4 (2012).

[19] O.A. Jaramillo, E. Venegas-Reyes, J.O. Aguilar, R. Castrejón-García, F. Sosa-Montemayor, Parabolic trough concentrators for low enthalpy processes, Renew. Energy. 60 (2013) 529–539.

[20] G. Coccia, G. Di Nicola, M. Sotte, Design, manufacture, and test of a prototype for a parabolic trough collector for industrial process heat, Renew. Energy. 74 (2014) 727–736.

[21] S.M. Arsalan, V. Prakash, R. Francis, Performance Evaluation of Solar Parabolic Trough Collector with Stainless steel Sheet as a Reflector, Int. j. of Eng. Res. & Sci. vol. 2, no. 6, pp. 1–7, 2016.

[22] A.K. Pandey, A.K. Rai, V. Sachan,"Design fabrication and performance evaluation of a low cost parabolic trough collector with copper receiver ,International journal of mechanical engineering and technology. vol. 5, no. 5, pp. 8–14, 2014.

[23] V. Arora, T. Sheorey, Development and Performance Characteristics of a Low-Cost Parabolic Solar Collector, 2nd Int. Conf. Power Energy Syst. (ICPES 2012). 56 (2012) 80–84.

[24] ANSI/ASHRAE 93-1986 (RA 91). Methods of testing to determine the thermal performance of solar collectors. American Society of Heating, Refrigerating and Air-Conditioning Engineers,Inc.;1991.

[25] Sukhatme, S.P. 1999. Solar Energy – Principles of thermal collection and storage- Second edition. New Delhi: Tata McGraw-Hill Publishing Company Limited.

[26] Gary Jorgensen, Reflective Coatings for Solar application, NREL, Prepared for the Society of Vacuum Coaters, 36th Annual Technical ,Conference, April 27-29, 1993..

[27] Kalogirou S. Solar energy engineering: processes and systems. USA: Academic Press; 2009.

[28] Holman JP. Experimental methods for engineers. 6th ed. Singapore: McGrawHill Book Co.; 1994.

[29] IS 875 (Part-III).Indian standard code of practice for design loads for building and structures.2nd revision,1987.

[30] I.H. Yilmaz, M.S. Söylemez, Thermo-mathematical modeling of parabolic trough collector, Energy Convers. Manag. 88 (2014) 768–784.

[31] İ. Halil, Modeling , simulation and performance analysis of parabolic trough solar collectors : A comprehensive review, 225 (2018) 135–174.

[32] S.K. Verma, N.K. Gupta, D. Rakshit, A comprehensive analysis on advances in application of solar collectors considering design, process and working fluid parameters for solar to thermal conversion, Sol. Energy. 208 (2020) 1114–1150.

[33] Duffie, J.A., Beckman, W.A., 2006. Solar engineering of thermal processes, 3rd ed. Wiley, New York. Esen, H., Esen, M. G.N. Tiwari, D. Atheaya, T. A, Review on solar thermal power concentrators, MOJ Sol.Photoenergy Syst. 1 (2017) 71–89.